

Soil aggregates and pore changes under raindrop splash

Guanglu Li¹, Yangyang Ren¹, Gangan Ma¹, Mingxi Yang¹, Yu Fu², Weiliang Hou¹, and Xudong Mu¹

¹Northwest A & F University

²Northwest A&F University

November 24, 2022

Abstract

Raindrop splash engenders the dispersion and transport of the soil particles, that is the primary stage in the process of soil erosion. Raindrops with different diameters may have different influences on different soil structures. The research objective was to quantitatively and visually analyze the change in surface aggregates and pore microstructure of five soils (Eum-Orthic Anthrosol, Ustalf, Cumulic Haplustoll, Ustochnept and Quartisamment) in the Loess Plateau caused by various raindrop diameters (2.67, 3.39 and 4.05 mm) using rainfall tests, synchrotron-based X-ray micro-computed tomography (SR- μ CT) and digital picture processing. Surface aggregate fragmentation and pore plugging rose as growing raindrop diameter. Under raindrop splash, the increase in raindrop diameter increased the number of microaggregates ($\leq 250 \mu\text{m}$) of Cumulic Haplustoll, Ustalf and Eum-Orthic Anthrosol; the irregular pore-shape factor of Quartisamment and Ustochnept; and the total number of aggregates and pores. Moreover, the soil physicochemical properties also had a significant impact on surface aggregate breakdown and pore plugging ($P < 0.01$). Higher sand contents made the soil structure of Quartisamment and Ustochnept more susceptible to splashing. The FD of Eum-Orthic Anthrosol, Ustalf and Cumulic Haplustoll were lower than those of Quartisamment and Ustochnept. The results showed that during rainfall, both raindrop diameter and soil properties affect surface aggregate stability and pore connectivity, which creates the material basis for forming surface crust, clogging pores and reducing the infiltration rate.

Hosted file

essoar.10509546.1.docx available at <https://authorea.com/users/343128/articles/602641-soil-aggregates-and-pore-changes-under-raindrop-splash>

Y. Y. Ren¹, G. L. Li^{1,2*}, G.G. Ma¹, M. X. Yang¹, Y. Fu², W. L. Hou¹, X. D. Mu¹

¹ College of Resources and Environment, Northwest A&F University, Yangling 712100, Shaanxi, China.

² Institute of Soil and Water Conservation, Northwest A&F University, Yangling 712100, Shaanxi, China.

Corresponding author: Guanglu Li (guangluli@nwsuaf.edu.cn)

Key Points:

- Soil aggregates and pore microstructure were investigated under different raindrops
- X-ray micro-computed tomography and digital picture processing were used
- The number of aggregates and pores increase with the increase in raindrop diameter
- Raindrop diameter and soil properties affect aggregate stability and pore connectivity.

Abstract

Raindrop splash engenders the dispersion and transport of the soil particles, that is the primary stage in the process of soil erosion. Raindrops with different diameters may have different influences on different soil structures. The research objective was to quantitatively and visually analyze the change in surface aggregates and pore microstructure of five soils (Eum-Orthic Anthrosol, Ustalf, Cumulic Haplustoll, Ustochnept and Quartisamment) in the Loess Plateau caused by various raindrop diameters (2.67, 3.39 and 4.05 mm) using rainfall tests, synchrotron-based X-ray micro-computed tomography (SR-CT) and digital picture processing. Surface aggregate fragmentation and pore plugging rose as growing raindrop diameter. Under raindrop splash, the increase in raindrop diameter increased the number of microaggregates ($> 250 \mu\text{m}$) of Cumulic Haplustoll, Ustalf and Eum-Orthic Anthrosol; the irregular pore-shape factor of Quartisamment and Ustochnept; and the total number of aggregates and pores. Moreover, the soil physicochemical properties also had a significant impact on surface aggregate breakdown and pore plugging ($P < 0.01$). Higher sand contents made the soil structure of Quartisamment and Ustochnept more susceptible to splashing. The FD of Eum-Orthic Anthrosol, Ustalf and Cumulic Haplustoll were lower than those of Quartisamment and Ustochnept. The results showed that during rainfall, both raindrop diameter and soil properties affect surface aggregate stability and pore connectivity, which creates the material basis for forming surface crust, clogging pores and reducing the infiltration rate.

1 Introduction

The soil structure comprises solid, liquid and gas phases (Young & Crawford, 2004), which can reflect the quality of soil. In addition, soil structure is the basis of maintaining soil function, which can determine the status of soil water and gas, nutrient supply and soil anti-erosion ability (Angers & Caron, 1998). Soil aggregate is the basic unit of soil structure, and its alinement and distribution will affect soil physical properties (Six & Paustian, 2014). While the characteristics of soil pore can veritably reflect the internal framework of soil structure, which can be used as the test index to directly and factually reflect the quality of soil structure (Rabot et al., 2018). Raindrop splash erosion destroys the surface soil structure, disperses soil particles, and causes pore plugging, which is the first step in water erosion. During the process of water erosion, the main reason for aggregate detachment is the mechanical damage caused by rainwater wetting and raindrop impact force (Le Bissionaais, 1996; Legout et al., 2005; Le Bissonnais, & Arrouays, 1997). Based on simulated rainfall experiments, Li et al. (2018), Fu et al. (2016) and Fu et al. (2017b) found that larger diameter raindrops can lead to a higher degree of aggregate breakdown and dispersion. Compared with in-situ soil, smaller soil particles will be generated due to aggregate breakdown, then these particles will replace the particles of original soil, and redirect a more consecutive structure, creating the surface seal (Ramos et al., 2003). This seal reduces surface soil porosity, and ultimately decreases the infiltration rate of surface soil and promotes runoff (Arjmand Sajjadi & Mahmoodabadi, 2015; Fu et al., 2016; Fu et al., 2020; Li et al., 2018).

Generally, the structural properties of soil (e.g., organic matter, clay, etc.) are also important factors affecting soil aggregate fragmentation. Previous studies have shown that aggregates with larger particle sizes and soils with higher organic matter content can reduce splash erosion and decrease the separation of soil particles (Ekwue, 1991). In addition, the lower the content of soil organic matter, the higher the susceptibility of crust (Ramos et al., 2003). Aggregate breakdown and dispersion were stronger in soils with a lower organic matter content (Lado, 2004). Furthermore, soil with a low sand content or a high clay content is also less affected by splash erosion (Dimitrova & Yanful, 2012; Fu et al., 2020). However, all of these studies approached the breakdown mechanism of soil aggregates from a macroscopic view, and there are few studies that observe and quantitatively analyze soil aggregates based on the internal microstructure of the aggregates, the sieving method will destroy the original soil structure to some degree, and it is difficult to observe the real distribution of pores in soil structure. Thus, quantitative and visual analysis of soil internal microstructure plays an important role in studying the change of soil structure under rainfall.

Conventionally the study of soil micromorphology is based on the observation of soil thin sections by electron microscopy to carry out two-dimensional microscopic morphology and quantitative analysis of soil (Pagliai, Vignozzi, & Pellegrini, 2004; Vogel, 1997). However, the fabrication process of soil samples is more tedious. Sharp tools such as knife are usually used to cut and process the air-dried samples to be studied. Next, right curing agents are also needed

for grinding and curing. Finally, the production of soil thin section was completed (Liu et al., 2016; Qin et al., 2009). In the process of making soil thin sections, due to the fragility of soil structure and the complexity of soil components, preparing soil sections requires much time, and only two-dimensional structural information on soil structure can be obtained from soil thin sections (Murphy, 1987), these will cause human disturbance to soil samples. Nowadays, in order to research various soil structures in a rapid and nondestructive manner, the adoption of synchrotron-based X-ray micro-computed tomography (SR-CT) is popular. This technique has the simultaneous advantages of relatively high contrast and resolution (Garbout et al., 2012; Taina et al., 2008) and can be used to study the micromorphology of soil structure. The images got by SR-CT technology are processed through image reconstruction, and then combined with digital image processing technology, the 3D microstructure of soil can be procured. Through quantitative analysis of the 3D microstructure in soil, nondestructive and comprehensive internal information of soil structure can be procured. Many scholars have studied the micromorphological characteristics of soil structure in different fields. Based on the non-destructive identification characteristics of SR-CT technology, soil aggregates (volume, surface area and sphericity) and pores (quantity, porosity and shape index) were quantitatively analyzed (Garbout et al., 2013; Yang et al., 2020). Through SR-CT technology, Ma et al. (2021), Starkloff et al. (2017) and Taina et al. (2013) and other scholars found that freeze-thaw cycles have negative effects on soil macropores and weaken the stability of soil aggregates. Moreover, some researchers found that the increase of organic matter enhanced the pore connectivity under different fertilization conditions and during the process of wasteland vegetation succession (Dal Ferro et al., 2013; Zhao et al., 2017; Hu et al., 2016).

Erosion capacity on the Loess Plateau has reached $37 \text{ Mg ha}^{-1} \text{ y}^{-1}$, it is one of the most severe regions in the world (Li & Pang, 2014). Rainfall erosion is the main driving force for dispersion and transportation of loess aggregates (Fu et al., 2016; Li & Pang, 2010; Wang et al., 2018). Rainfall erosion on the Loess Plateau has been studied; for example, taking Ustalf and Eum-Orthic Anthrosol as the research objects, Fu et al. (2017a) analyzed the discrepancy of fragmentation mechanism of different soil aggregates in the Loess Plateau. Their results showed that compared with Ustalf, the degree of splash for Eum-Orthic Anthrosol was lower for the identical raindrop diameter. Moreover, owing to secondary raindrop splash erosion, the fracture again of Eum-Orthic Anthrosol aggregate that causing a decline in soil fertility and soil productivity (Fu et al., 2020). Due to changes in climate and soil formation conditions on the Loess Plateau, the characteristics of various soil types are quite variable (Fu et al., 2020). About the study of soil erosion mechanisms have only focused on a single or a few soils, so that it restricts the comprehension of erosion condition in the Loess Plateau. In addition, the research of soil aggregate and pore plugging in the Loess Plateau under rainfall conditions from a microscopic perspective are rarely. Therefore, based on rainfall simulation experiments, the intentions of this research were to research (1) the changes in the 3D microstructure of surface soil

aggregates and pores under different rainfall conditions and (2) the differences in the 3D microstructure of surface aggregates and pores in different soil types on the Loess Plateau using synchrotron radiation micro CT and digital image processing. This research is significant because it allows a better understanding of the mechanisms by which the internal soil structure changes during the rainfall erosion process and because it addresses the issues of soil surface crust and infiltration that are caused by rainfall.

2 Materials and Methods

2.1 Soil sampling

Five soil types (distributed from south to north according to latitude) on the Loess Plateau were studied (Table 1). According to USDA, these soils are Eum-Orthic Anthrosol, Ustalf, Cumulic Haplustoll, Ustochnept and Quartisamment, respectively. The location of specific sampling points is shown in Figure 1. The description of each sampling point is shown in Table 1. Five sampling points belonged to traditional agricultural planting areas in China. Maize (*Zea mays* Linn.) and wheat (*Triticum aestivum* L.) as principal crops.

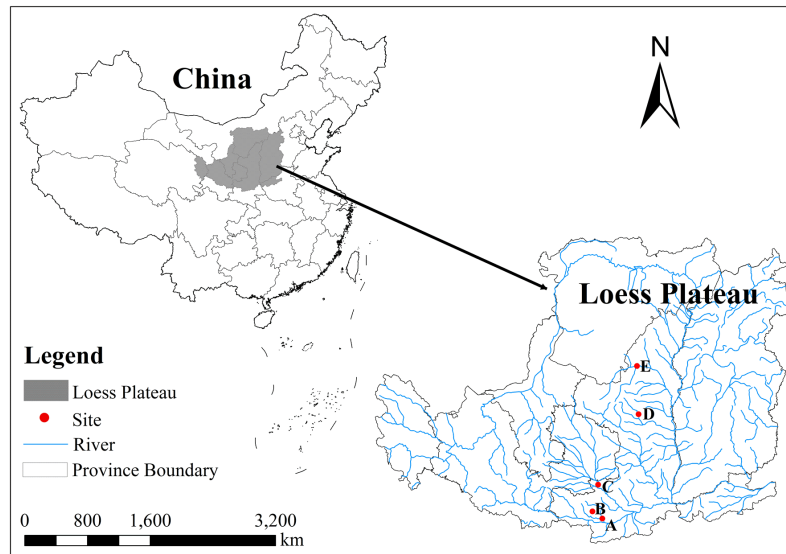


Figure 1. Location map of soil sampling points. (Notes: (A) represent Eum-Orthic Anthrosol, (B) represent Ustalf, (C) represent Cumulic Haplustoll, (D) represent Ustochnept and (E) represent Quartisamment.) (Fu, Yang, et al., 2020). Data source: Geospatial Data Cloud site, Computer Network Information Center, Chinese Academy of Sciences (<http://www.gscloud.cn>). This figure was created via ArcMap 10.2 (<http://www.esri.com/>).

Dry branches and fallen leaves were removed from the surface layer before sampling, and a cutting ring (diameter was 10 cm and height was 5cm) was used to gather the undisturbed surface soil (0 to 20 cm) samples through the diagonal

method. Each soil sample gathered 36 cutting ring samples, 180 samples were collected in all. According to Wang et al. (2018), in order to attain the bulk density, the round knife method was adopted, the organic matter was measured through potassium dichromate heating method, the total nitrogen (N) and total phosphorus (P) were analyzed via Kjeldahl N and HClO₄-H₂SO₄ method, respectively, and the mechanical composition was obtained with a Malvern laser particle size analyzer. The basic physicochemical properties are shown in Table 1.

Table 1. Basic situation of sampling points and basic soil physicochemical properties

@	>p(- 22)	* >p(- 22)	* >p(- 22)	* >p(- 22)	* >p(- 22)	* >p(- 22)	* >p(- 22)	* @ sites	& Soil type	& longitudes	& latitudes	& Annual average temperature /°C	& Annual average precipitation /mm	& Bulk density/(g · cm ⁻³)	& Soil organic/%	& Total nitrogen/(g/kg)	& Total phosphorus/(g/kg)	& Soil mechanical compositions	& Sand/%	& (2~0.02mm)	& silt/%	& (0.02~0.002mm)	& clay/%	& (0.002mm)
Yangling	& Eum-Orthic Anthrosol	& 108°03	& 29 E,	& 34°18	& 24 N	& 13.00	& 660.00	& 1.37	& 1.46	& 1.04	& 0.62	& 33.26	& 44.07	& 22.67										
Meixian	& Ustalf	& 107°45	& 36 E,	& 34°29	& 24 N	& 12.90	& 609.50	& 1.29	& 1.33	& 0.87	& 0.83	& 45.96	& 41.06	& 12.98										
Changwu	& Cumulic Haplustoll	& 107°40	& 59 E,	& 35°14	& 27 N	& 9.10	& 580.00	& 1.12	& 1.55	& 0.95	& 0.70	& 52.31	& 37.44	& 10.25										
Ansai	& Ustochnept	& 109°19	& 23 E,	& 36°51	& 30 N	& 8.80	& 500.00	& 1.18	& 0.9	& 0.43	& 1.40	& 72.82	& 21.56	& 5.62										
Jingbian	& Quartisamment	& 109°20	& 15 E,	& 38°03	& 15 N	& 7.80	& 395.40	& 1.46	& 0.41	& 0.22	& 0.80	& 81.80	& 14.55	& 3.65										

2.2 Rainfall test

This experiment used the device of needle-head simulated rainfall. It comprised raindrop generator and collecting device. The raindrop generator was a drop-type, composing of a cylindrical box, and it was open-top (diameter was 10 cm and height was 10 cm). Bottom of the box arranged 21 injector needles at 2 cm intervals, including US needles sizes of 7, 12 and 16. In order to control the raindrop diameter, the needle size needs to be adjusted (Table 2) (Fu et al., 2016). The stainless steel plate formed the collecting device for the splashed soils (the diameter was 110 cm). Throughout the experiment, in order to avoid disturbance from crossflow, around the experiment equipment placed the plastic wrap (Fu et al., 2016). For each raindrop diameter, the rainfall period

was 10 minutes with three replications, that is, for each raindrop diameter, the total number of raindrops impacts in the experimental treatments was three. The specific test methods and test devices are shown in Fu et al. (2017a). The specific rainfall experimental parameters are shown in Table 2. During the experiment, three raindrop diameters were selected (2.67mm, 3.39mm and 4.05mm). These raindrop diameters belong to the range of raindrop diameter in natural rainfall. Its corresponding rainfall kinetic energy and rainfall intensity are shown in Table 2, these parameters are corresponding with the rainfall features on the Loess Plateau (Jiao, 1999). The specific calculation procedures are shown in Yang et al. (2020).

Table 2. Rainfall experiment parameters

Rainfall experiment parameters			
Needle size	7	12	16
Falling height / m	2	2	2
Raindrop diameter / mm	2.67	3.39	4.05
Terminal speed / m s⁻¹	5.36	5.48	5.54
Rainfall kinetic energy / J m⁻² s⁻¹	2.41×10 ⁻⁵	5.15×10 ⁻⁵	8.97×10 ⁻⁵
Rainfall intensity / mm h⁻¹	5.76	68.61	217.26

2.3 CT scanning and image processing

Before image scanning, soil samples inside the cutting ring were air-dried. Before and after each rainfall event, dry soil clods (2 cm length × 2 cm width) were obtained from the splashed soil surface layer (depth 0.5 cm) using a knife. The soil blocks were kept in containers with sponges to maintain their structural integrity (Yang et al., 2020). 54 dry soil blocks were selected for CT scanning from each soil for a total of 270 samples. Image scanning was taking place in synchrotron-based X-ray micro-computed tomography (SR-CT) that belongs to the BL13W1 beam line of the Shanghai Synchrotron Radiation Facility (SSRF). For purpose of image reconstruction, the Phase-sensitive X-ray image processing and tomography reconstruction software (PITRE) was applied. Nearly 1500-2000 gray scale images (1052 × 1052 pixels) with a 32-bit TIFF format were reconstructed using the back-projection algorithm. Finally, the image was converted into an 8-bit TIFF format for subsequent processing. Each voxel presented 3.25 m cubic volume.

ImagePy v0.2 was an open-source software, it was used to perform the image processing, visualization and quantitative analysis (Yang et al., 2020; Wang et al., 2018). In order to further image analysis, Sub-volumes of 512 cubic voxels (viz., 1.664 mm cubic volume) were extracted to show inscribed cubes of aggregates. That can avoid edge effects and the effects of soil depth. In the process of binary imaging, the automatic Otsu algorithm was used to segment the gray images, it belongs to the global threshold method (Zhao et al., 2017; Zhao, Xu et al., 2017). Furthermore, in order to obtain the threshold value,

visual observation and reiterated debugging were also vital (Yang et al., 2020). Because of the constraints of image resolution, only aggregates and pores larger than 3.25 μm could be identified and studied. Finally, the 3D aggregates and pores were visualized and quantitatively analyzed using Viewer 3D and Analysis 3D of ImagePy v0.2, respectively.

2.4 Data analysis

After image processing, the soil structure divided into soil aggregates (white) and pores (black) in the binary image. However, soil aggregates and pores have varied morphology and sizes, so the number of pixels in each aggregate or pore is also different. Six-neighborhood connectivity method was used for quantitative analysis of aggregates and pores in image processing (Yang et al., 2020). Based on Up Down Watershed 3D of ImagePy v0.2, the soil aggregate was segmented by watershed segmentation algorithm.

At present, there are few studies on the classification of soil aggregates from the viewpoint of digital image, and the classification criteria of soil pores is not strict. Therefore, in the test, the soil aggregates were classified into five size classes: > 500 , 250-500, 106-250, 53-106, and ≤ 53 μm based on their cementation type and size. According to the type of binders and aggregate diameter, soil aggregates were divided into macroaggregates (> 250 μm) and microaggregates (≤ 250 μm). The quality of soil structure can be judged through the number of water-stable aggregates (> 250 μm). On the basis of the equivalent diameter of the pores, the soil pores were classified into six size classes: > 1000 , 100-1000, 75-100, 50-75, 25-50, and ≤ 25 μm . In line with capillary potential of soil pores, soil pores were divided into macropores (> 100 μm) (Luxmoore, 1981) and small pores (≤ 100 μm). The distribution characteristics of surface soil aggregates and pores were represented by the relative quantity percentage (i.e., the number of aggregates or pores of the same particle size in the soil out of the total number of aggregates or pores) and the relative volume percentage or relative porosity (namely, the volume of aggregates or pores of the same particle size in the soil out of the total volume of aggregates or pores).

The aggregate or pore-shape factor was used to describe the morphological changes in surface soil aggregates and pores under raindrop splash (Lars J. Munkholm 2016). The calculation was based on equation (1):

(1)

In the equation, V and A express the actual volume and actual superficial area of the measured aggregate or pore, respectively. Where F belongs between 0 and 1. When the research object is aggregates, the larger the F , the more regular and spherical the aggregate shape; the smaller the F , the more irregular the aggregate shape. According to Yang et al. (2020), Zhou et al. (2012), when the research object is pores, the soil pores were divided into three kinds of morphology as regular pore ($F \geq 0.5$), irregular pore ($0.2 < F < 0.5$) and elongated pore ($F \leq 0.2$).

The 3D mass fractal dimension (FD) of soil aggregates was calculated by the BoneJ plug-in in ImageJ1.52p (<http://imagej.nih.gov/ij>) software. The FD can represent the geometric fractal characteristics of objects, self-similarity and scale-independence (Dal Ferro et al., 2013). It was got through box-counting method. That is, using cube box with different sides to cover the image stack, and record the number of boxes (Perret et al., 2003). The lower the FD is, the better the stability of soil aggregates is (Gong & Yu Rong, 2001). The calculation was based on equation (2):

(2)

In the equation, N () represents the number of boxes, s represents the side length of the box.

For sake of carrying out data processing and chart drawing, Microsoft Excel 2010 and Origin 2018 were adopted. At 5% significance level, the variance analyses (one-way analysis of variance [ANOVA], Two-way ANOVA and multivariable variance analysis [MANOVA]), correlation analysis and multiple comparisons (least significant difference [LSD]) were performed by SPSS 18.0 statistical analysis software.

3 Results

3.1 The 3D microstructure analysis of soils

It can be observed that from the 2D micrograph, soil aggregates and pores changed in response to raindrop splashes with different diameters (Figure 2). For unsplashed soil, the soil aggregate structure was compact. Under the impact of 2.67 mm raindrops, soil aggregates began to break down; the trend was more obvious in larger aggregates. Under the impact of 3.39 mm raindrops, small aggregates gathered around the large aggregates, and more small pores appeared between the aggregates. Under the impact of 4.05 mm raindrops, small aggregates gathered to form dense, large aggregate structures, and the small pores between the aggregates became increasingly clear. These phenomena were also observed in the 3D aggregate microstructure (Figure 3). In addition, among the five soil pores, the small pores were mostly isolated, and the macropores were mostly continuous structures. With increasing raindrop diameter, the number of small pores increased, and the connectivity of macropores decreased (Figure 4).

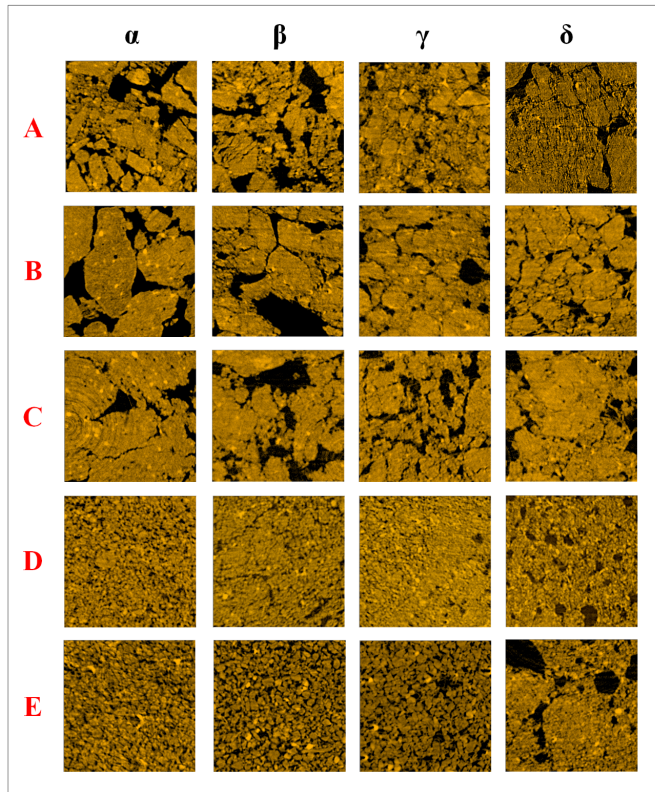


Figure 2. Two-dimensional microstructure changes in soil aggregates (yellow) and pores (black) under raindrop splash (1.664 mm length \times 1.664 mm width). (Notes: (A) represent Eum-Orthic Anthrosol, (B) represent Ustalf, (C) represent Cumulic Haplustoll, (D) represent Ustochnept and (E) represent Quartisamment. - represent unsplashed soil, soil splashed by 2.67 mm raindrops, soil splashed by 3.39 mm raindrops and soil splashed by 4.05 mm raindrops.)

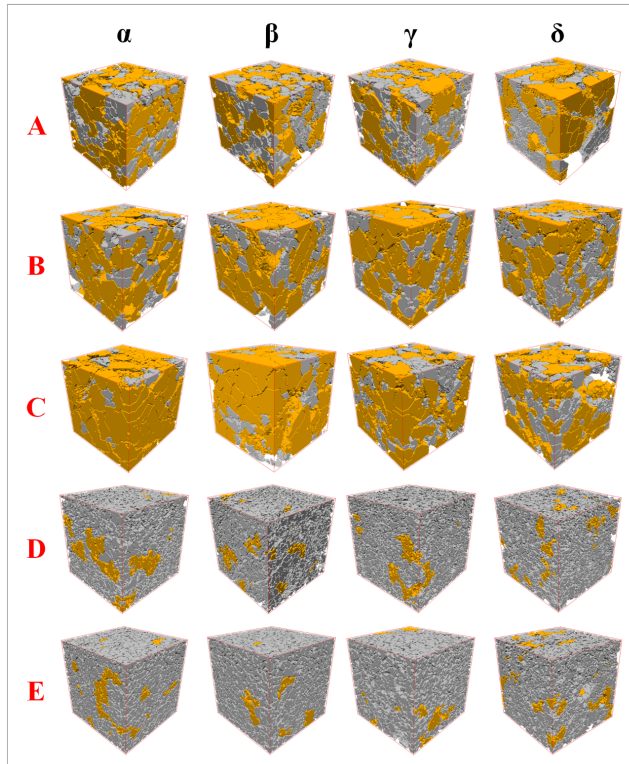


Figure 3. Three-dimensional microstructure changes in soil aggregates under raindrop splash (the length, width and height are all 1.664 mm). (Notes: The yellow part represents macroaggregates ($> 250 \mu\text{m}$), and the gray part represents microaggregates ($< 250 \mu\text{m}$). (A) represent Eum-Orthic Anthrosol, (B) represent Ustalf, (C) represent Cumulic Haplustoll, (D) represent Ustochnept and (E) represent Quartisamment. - represent unsplashed soil, soil splashed by 2.67 mm raindrops, soil splashed by 3.39 mm raindrops and soil splashed by 4.05 mm raindrops.)

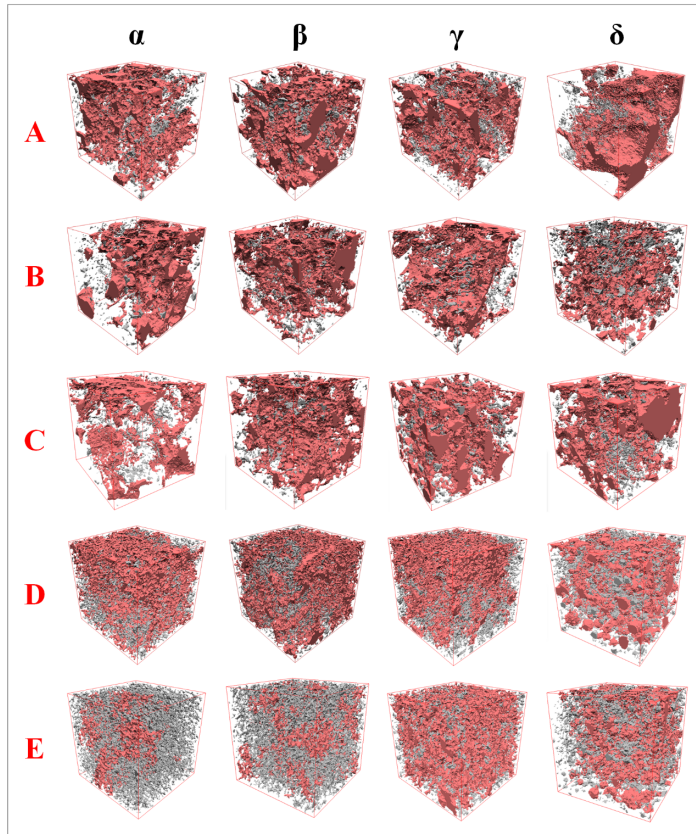


Figure 4. Three-dimensional microstructure changes in soil pores under raindrop splash (the length, width and height are all 1.664 mm). (Notes: The pink part represents macropores ($> 100 \mu\text{m}$), and the gray part represents small pores ($< 100 \mu\text{m}$). (A) represent Eum-Orthic Anthrosol, (B) represent Ustalf, (C) represent Cumulic Haplustoll, (D) represent Ustochnept and (E) represent Quartisamment. - represent unsplashed soil, soil splashed by 2.67 mm raindrops, soil splashed by 3.39 mm raindrops and soil splashed by 4.05 mm raindrops.)

It is reflected by the Figure 2,3 and 4 that the microstructure was different in the different soils. It is similar for the structure of aggregate and pore in Cumulic Haplustoll, Ustalf and Eum-Orthic Anthrosol (Figure 2 & Figure 3). The structure was mainly composed of macroaggregates with irregular shapes, and macroaggregates were most abundant in the Cumulic Haplustoll. Moreover, compared with Ustochnept and Quartisamment, the macropores of these three soils were more continuous and connected (Figure 4). However, the structures of Ustochnept and Quartisamment were similar (Figure 3). The structure of those soils was mainly composed of regularly-shaped microaggregates.

Before and after raindrop splash, the FD of each soil changes as shown in Fig-

ure 5. On the whole, the FD are between 2 and 3. The FD of Eum-Orthic Anthrosol, Ustalf and Cumulic Haplustoll were lower than those of Quartisamment and Ustochnept. The FD of Cumulic Haplustoll reached the lowest value (mean: 2.72051402), the FD of Ustochnept reached the highest value (mean: 2.933258392). From Figure 5, the FD of each soil increased compared with that of unsplashed soil under splashed by raindrop size of 3.39mm. The FD of Cumulic Haplustoll, Ustochnept and Quartisamment decreased under splashed by raindrop size of 4.05mm.

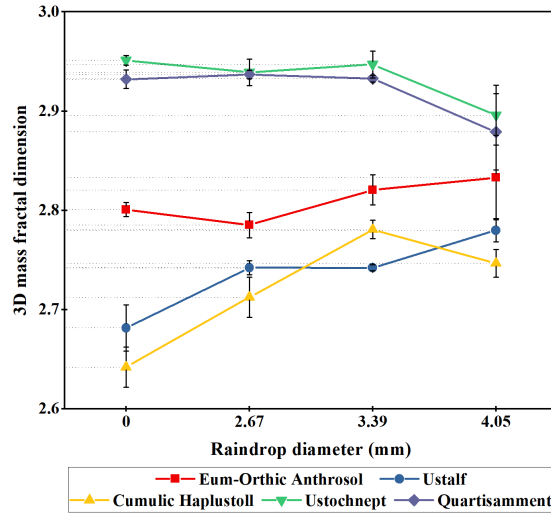


Figure 5. 3D mass fractal dimension of soil aggregates.

3.2 Effects of raindrop splash on the number of soil aggregates and pores

After impact by raindrop, the amount of aggregates and pores changed. In rainfall erosion, the influence of soil type and raindrop diameter upon the total number of aggregates and pores were significant ($P < 0.05$) (Table 3). As raindrop diameter increased, the total quantity of aggregates and pores in five soil surface layers increased. In addition, the number of pores was greater than that of aggregates (Figure 6A, B). Raindrop splashing later, the total number of aggregates were ranked as Quartisamment > Ustochnept > Eum-Orthic Anthrosol > Ustalf > Cumulic Haplustoll (Figure 5A), and the total number of pores were ranked as Ustochnept > Quartisamment > Eum-Orthic Anthrosol > Ustalf > Cumulic Haplustoll (Figure 6B). In Eum-Orthic Anthrosol and Ustalf, to compare and contrast with unsplashed soil aggregates and other splashed soil aggregates, the total number of aggregates in soil splashed by 4.05 mm raindrops differed significantly ($P < 0.05$) (Figure 6A). Under the same rainfall conditions, the total number of aggregates in Ustochnept and Quartisamment differed significantly from those in the other three soils ($P < 0.05$) (Figure 6A). Besides Ustalf, the total number of soil pores in soils splashed by 4.05 mm raindrops

was significantly different from those of the unsplashed soil and other splashed soils ($P < 0.05$) (Figure 6B).

Table 3. Multivariable variance analysis of soil types and raindrop diameters on the number of aggregates and pores ($P < 0.05$)

@ >p(- 10) * @

Source	Type III Sum of Squares	df	Mean Square	F	Sig.
Corrected Model	5.709E7 ^a	19	3004530.516	26.062	.000
					4.777E8 ^b

&
19
&
2.514E7
&
18.437
&
.000

Intercept
&
9.469E7
&
1
&
9.469E7
&
821.378
&
.000
&
1.270E9
&
1
&
1.270E9
&
931.595
&

.000

Raindrop Diameter

&

5.369E7

&

4

&

1.342E7

&

116.439

&

.000

&

1.399E8

&

4

&

3.498E7

&

25.652

&

.000

Soil Type

&

2151357.000

&

3

&
717119.000

&
6.221

&
.001

&
2.120E8

&
3

&
7.067E7

&
51.828

&
.000

Raindrop Diameter * Soil Type

&
1240997.375

&
12

&
103416.448

&
.897

&
.555

&

1.257E8
&
12
&
1.048E7
&
7.685
&
.000

Error
&
6916972.000
&
60
&
115282.867
& &
&
8.181E7
&
60
&
1363573.738
& &

Total
&
1.587E8
&
80

& & &
 &
 1.830E9
 &
 80
 & & &

 Corrected Total
 &
 6.400E7
 &
 79
 & & &
 &
 5.595E8
 &
 79
 & & &

Dependent Variable: a. Total number of aggregates; b. Total number of pores
 a. R Squared = 0.892 Adjusted R Squared = 0.858
 b. R Squared = 0.854 Adjusted R Squared = 0.807

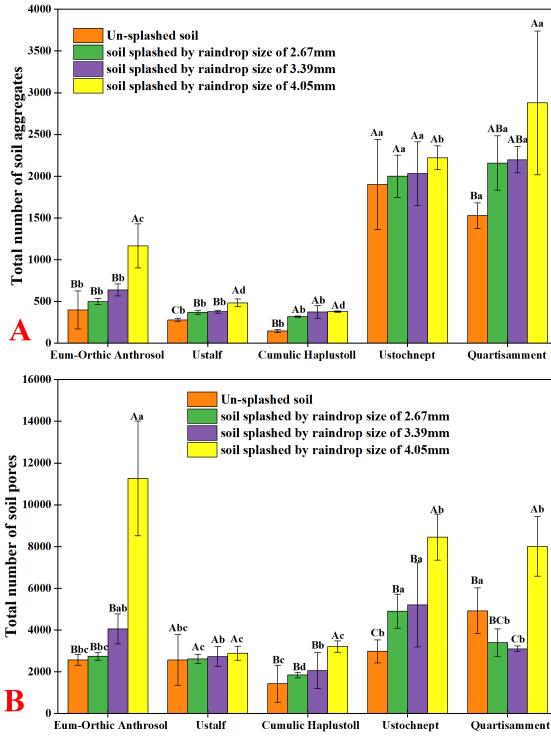


Figure 6. Quantitative change characteristics of aggregates (A) and pores (B) under raindrop splash. (Notes: Differences in the various raindrop diameters and the same soil types are represented by uppercase letter at 5% significant level. Differences in the various soil types and the same raindrop diameters are represented by lowercase letter at 5% significant level) .

3.3 Effects of soil physicochemical properties on the number of soil aggregates and pores

Under raindrop splash, the discrepancy of amounts in surface aggregate and pore could be caused by the differences of the physical and chemical characteristics in un-splashed soil. As the organic matter, silt and clay contents increased, the amount of surface soil aggregate and pore decreased as a whole (Figure 7A, D & E). Overall, the amount of pores rose with increasing bulk density (Figure 7B). The overall number of aggregates and pores decreased with increasing sand content (Figure 7C). The number of aggregates corresponding to organic matter contents of 0.41% and 0.9%, bulk densities of $1.18 \text{ g} \cdot \text{cm}^3$ and $1.46 \text{ g} \cdot \text{cm}^3$, sand contents of 72.82% and 81.8%, silt contents of 14.55% and 21.56% and clay contents of 3.65% and 5.62% were significantly higher than those corresponding to other contents ($P < 0.05$). The number of pores corresponding to an organic matter content of 0.41%, bulk density of $1.46 \text{ g} \cdot \text{cm}^3$, sand content of 81.8%, silt content of 14.55% and clay content of 3.65% were significantly higher than

those corresponding to other contents ($P < 0.05$).

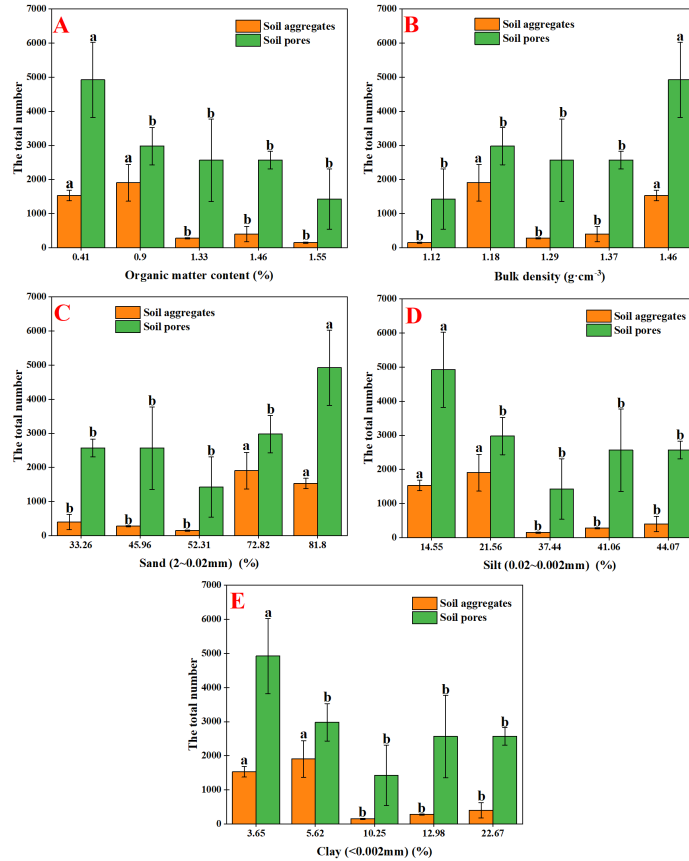


Figure 7. The relationship between soil properties and the amount of aggregate and pore. (Notes: A-E represent organic matter, bulk density, sand, slit and clay, respectively. Differences in the various soil types, differences between aggregates and differences between pores are represented by small letter at 5% significant level.)

3.4 Effect of raindrop splash on soil aggregates and pores

From the quantity distribution chart of soil aggregates and pores, microaggregates ($> 250 \mu\text{m}$) and small pores ($< 100 \mu\text{m}$) are the major part in soil structure (Figure 8A & Figure 9A). Among them, the microaggregates mainly consisted of 106-250 μm aggregate fragments, and surface soil pores were mainly composed of small pores ($< 100 \mu\text{m}$), 99% of which were small pores $< 25 \mu\text{m}$. It can be seen in Figure 8 that the particle size distribution (quantity or volume) of aggregates in Eum-Orthic Anthrosol, Ustalf and Cumulic Haplustoll differ greatly from those in Ustochnept and Quartisamment. In Ustochnept and Quartisamment, there were no aggregate fragments $> 500 \mu\text{m}$ (Figure 8), the relative quantity per-

centage of microaggregates were 96.22-98.45% and 97.20-99.31%, respectively (Figure 8A).

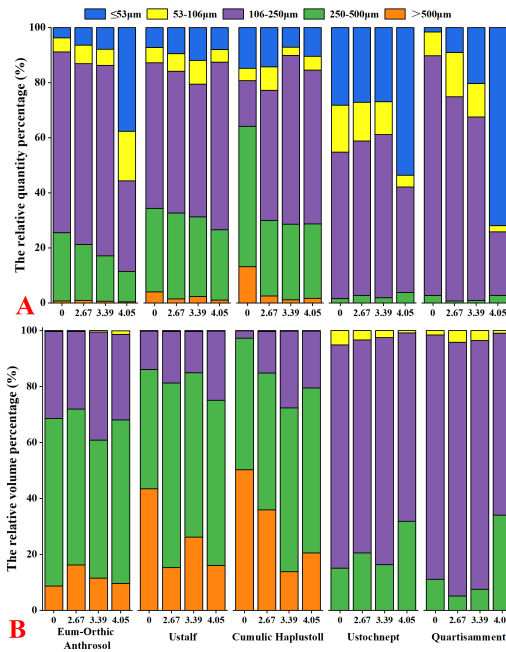


Figure 8. Relative quantity percentage (A) and relative volume percentage (B) of soil aggregate size classifications under raindrop splash. (Notes: 0 represents unsplashed soil, 2.67 represent soil splashed by raindrops of 2.67 mm, 3.39 represent soil splashed by raindrops of 3.39 mm and 4.05 represent soil splashed by raindrops of 4.05 mm.)

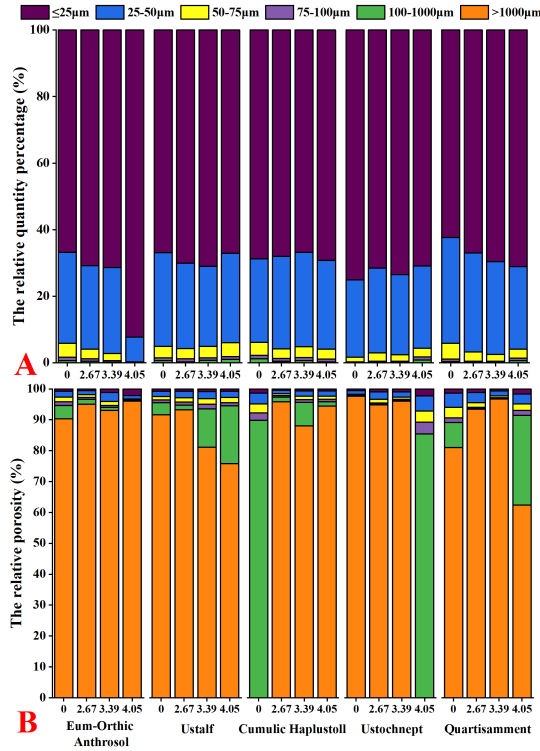


Figure 9. Relative quantity percentage (A) and relative porosity (B) of soil pore size classifications under raindrop splash. (Notes: 0 represents unsplashed soil, 2.67 represent soil splashed by raindrops of 2.67 mm, 3.39 represent soil splashed by raindrops of 3.39 mm and 4.05 represent soil splashed by raindrops of 4.05 mm.)

From the volume distribution chart of soil aggregates and pores, macropores ($> 100 \text{ m}$) are the major part in soil structure (Figure 8A & Figure 9A). Eum-Orthic Anthrosol, Ustalf and Cumulic Haplustoll were mainly comprised of large aggregates, the relative volume percentages were 60.77-71.93%, 75.03-86.05% and 72.35-97.30%, respectively (Figure 8B). Microaggregates still predominated in Ustochnept and Quartisamment (Figure 8B). The influence of soil type upon the $>106 \text{ m}$ aggregate fragments were significant ($P < 0.05$) (Table 4). The influence of soil type and raindrop diameter upon the macropores ($> 100 \text{ m}$) were significant ($P < 0.05$) (Table 5). Under different rainfall conditions, the relative porosity of macropores ($> 100 \text{ m}$) in Eum-Orthic Anthrosol, Ustalf, Cumulic Haplustoll, Quartisamment and Ustochnept was 94.04-96.71%, 93.56-95.59%, 89.89-97.40%, 89.14-96.93% and 85.39-97.77%, respectively, and was mainly composed of macropores ($> 1000 \text{ m}$).

Table 5. Two-way ANOVA of soil types and raindrop diameters on the relative porosity of aggregates ($P < 0.05$).

@ >p(- 12) * @

Source

&

Dependent Variable

&

Type III Sum of Squares

&

df

&

Mean Square

&

F

&

Sig.

Corrected Model

&

>1000

&

6.343^a

&

19

&

.334

&

2.965

&

.001

&

100-1000
&
4.881^b
&
19
&
.257
&
6.213
&
.000
&
75-100
&
.023^c
&
19
&
.001
&
1.105
&
.370
&
50-75
&
.054^d
&
19

&
.003
&
.762
&
.740
&
25-50
&
.280^e
&
19
&
.015
&
.767
&
.734
&
25
&
.267^f
&
19
&
.014
&
.942
&

.537

Intercept

&

>1000

&

38.802

&

1

&

38.802

&

344.667

&

.000

&

100-1000

&

2.036

&

1

&

2.036

&

49.251

&

.000

&

75-100

&
.019
&
1
&
.019
&
17.667
&
.000
&
50-75
&
.075
&
1
&
.075
&
20.027
&
.000
&
25-50
&
.315
&
1
&

.315
&
16.437
&
.000
&
25
&
.098
&
1
&
.098
&
6.581
&
.013

Raindrop
Diameter
&
>1000
&
2.241
&
3
&
.747
&

6.634
&
.001

&
100-1000
&
1.196
&
3
&
.399
&
9.643
&
.000

&
75-100
&
.005
&
3
&
.002
&
1.581
&
.203

&
50-75

&
.010
&
3
&
.003
&
.880
&
.457
&
25-50
&
.035
&
3
&
.012
&
.610
&
.611
&
25
&
.066
&
3
&

.022
&
1.462
&
.234

Soil Type
&
>1000
&
.966
&
4
&
.241
&
2.145
&
.086

&
100-1000
&
.730
&
4
&
.182
&
4.413

&
.003
&
75-100
&
.002
&
4
&
.001
&
.531
&
.713
&
50-75
&
.010
&
4
&
.003
&
.669
&
.616
&
25-50
&

.102
&
4
&
.025
&
1.328
&
.270
&
25
&
.063
&
4
&
.016
&
1.048
&
.390

Raindrop Diameter * Soil Type

&
>1000
&
3.137
&
12

&
.261
&
2.322
&
.016
&
100-1000
&
2.955
&
12
&
.246
&
5.956
&
.000
&
75-100
&
.015
&
12
&
.001
&
1.177
&

.320
&
50-75
&
.034
&
12
&
.003
&
.764
&
.684
&
25-50
&
.143
&
12
&
.012
&
.620
&
.817
&
25
&
.139

&
12
&
.012
&
.777
&
.671

Error
&
>1000
&
6.755
&
60
&
.113
& &
&
100-1000
&
2.480
&
60
&
.041
& &
&
75-100
&

.065
&
60
&
.001
& &
&
50-75
&
.226
&
60
&
.004
& &
&
25-50
&
1.151
&
60
&
.019
& &
&
25
&
.896
&
60
&
.015

& &

Total

&

>1000

&

51.900

&

80

& & &

&

100-1000

&

9.397

&

80

& & &

&

75-100

&

.107

&

80

& & &

&

50-75

&

.356

&

80

& & &

&

25-50
&
1.747
&
80
& & &
&
25
&
1.262
&
80
& & &

Corrected Total
&
>1000
&
13.098
&
79
& & &
&
100-1000
&
7.361
&
79
& & &
&
75-100
&

.088
 &
 79
 & & &
 &
 50-75
 &
 .280
 &
 79
 & & &
 &
 25-50
 &
 1.431
 &
 79
 & & &
 &
 25
 &
 1.164
 &
 79
 & & &

Dependent Variable: The particle size of soil aggregates (m).

- a. R Squared = 0.484 (Adjusted R2 = 0.321);
- b. R Squared = 0.663 (Adjusted R2 = 0.556);
- c. R Squared = 0.259 (Adjusted R2 = 0.025);
- d. R Squared = 0.194 (Adjusted R2 = -0.061);
- e. R Squared = 0.195 (Adjusted R2 = -0.059);

f. R Squared = 0.230 (Adjusted R2 = -0.014) (P<0.05)

Under raindrop splash, the morphology of aggregates and pores in soil surface changed (Figure 10 & Figure 11). Under the same rainfall conditions, Except for the unsplashed soil of Cumulic Haplustoll, the aggregate-shape factor first increased and then decreased with decreasing aggregate size, and the macroaggregate-shape factor was less than that of the microaggregates (Figure 10). The pore-shape factor increased with decreasing pore diameter. The macropore-shape factor was less than that of the small pores (Figure 11). The shape factor of the 25 μm pores had a maximal value, and the shape factor of the > 1000 μm aggregate fragments had a minimal value.

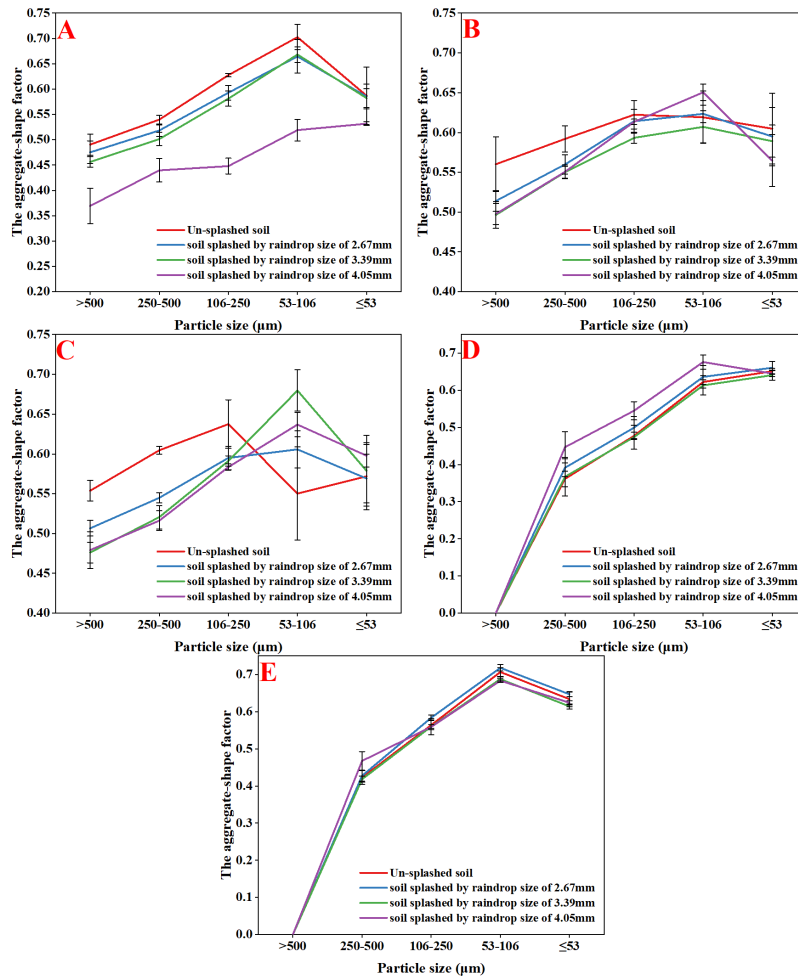


Figure 10. Morphological changes in soil aggregates under raindrop splash. (Notes: (A) represent Eum-Orthic Anthrosol, (B) represent Ustalf, (C) represent Cumulic Haplustoll, (D) represent Ustochnept and (E) represent Quarti-

samment.)

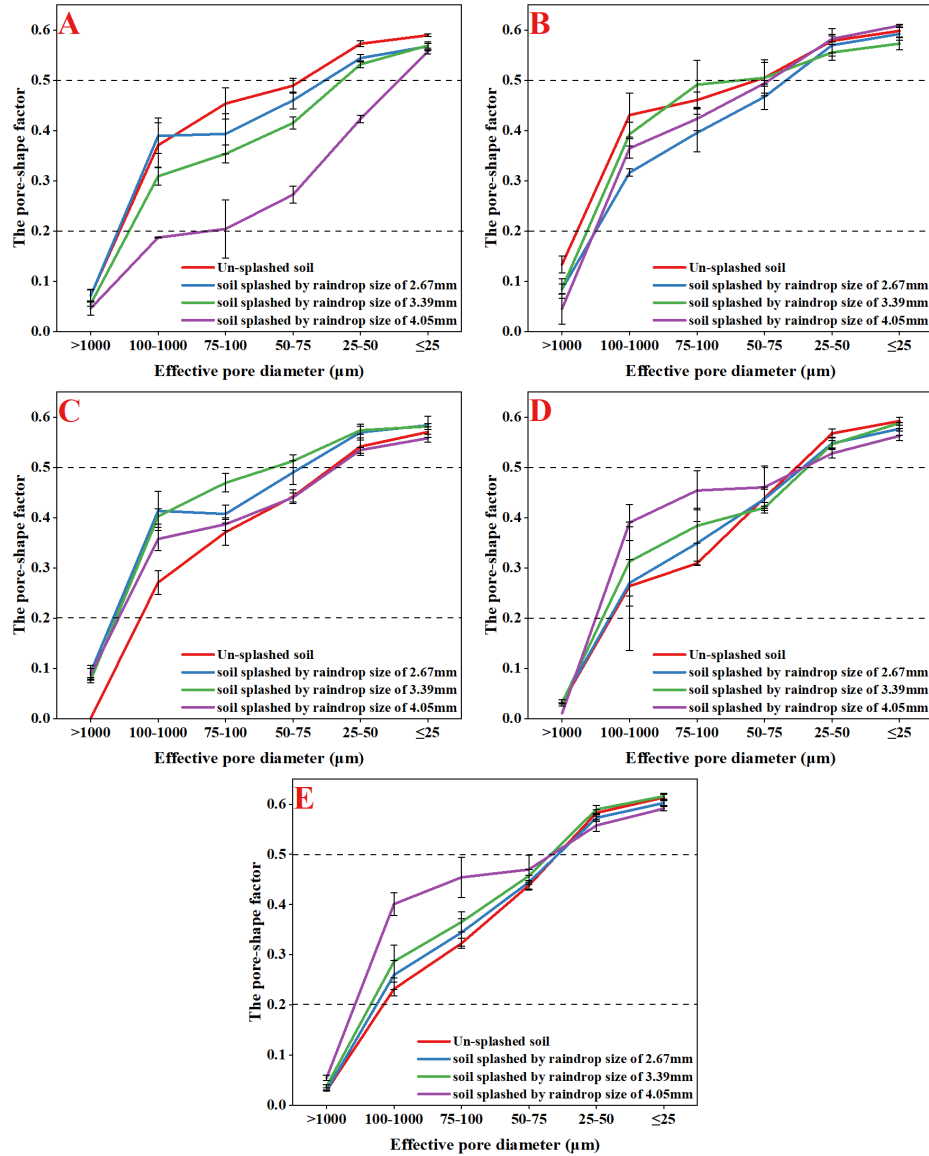


Figure 11. Morphological changes in soil pores under raindrop splash. (Notes: (A) represent Eum-Orthic Anthrosol, (B) represent Ustalf, (C) represent Cumulic Haplustoll, (D) represent Ustochnept and (E) represent Quartisamment.)

The shape factor of the 53-106 μm aggregate fragments had a maximal value and were nearly spherical. The shape factor of the $> 500 \mu\text{m}$ aggregate fragments had a minimal value and were irregular. In Ustochnept and Quartisamment, there

was little change in the aggregate-shape factor of different particle sizes before and after raindrop splash (Figure 10D, E). Pore diameter >1000 μm corresponds to elongated pore; pore diameter 50-1000 μm corresponds to irregular pore; and when the pore diameter ≤ 50 μm , the pore shape was regular. In Ustochnept and Quartisamment, compared with splashed soil, the irregular pore-shape factor of unsplashed soil was lower, and the pore shape factor increased with increasing raindrop diameter (Figure 11D, E).

4 Discussion

4.1 Quantity and volume distribution characteristics of soil structure under different rainfall conditions

With increasing raindrop diameter, the total number of surface soil aggregates and pores increased (Figure 6). The influence of soil type and raindrop diameter upon the total number of aggregates and pores were significant ($P < 0.05$). when the diameter of raindrop arrived at 4.05 mm, the total number of aggregates and pores reached their maximum. This conclusion indicates that for the soil aggregate breakdown and pore plugging, the raindrop diameter is one of the influencing factors, and the effect increases with increasing raindrop diameter. This is coincident with the experimental results of Fu et al. (2017a), who stated that large raindrops were the main power source for aggregate breakdown and dispersion in a rainfall event. Cumulic Haplustoll, Ustalf and Eum-Orthic Anthrosol was less affected by splashing than Quartisamment and Ustochnept (Figure 6). This may be explained by the higher organic matter, silt and clay contents of these three soils (Table 1) and the more stable soil structure. Aggregate breakdown and pore plugging caused by raindrop impacts depend not only on rainfall factors but also on soil erodibility (Li et al., 2018). However, soil erodibility is related to soil physicochemical characteristics, for example, organic matter, clay, and CaCO_3 contents and the proportion of exchangeable sodium (Lado 2004). After raindrop splash, the relationship between the number of aggregates and clay, silt and organic matter was remarkably negative correlation ($P < 0.01$), and was remarkably direct correlated with sand content ($P < 0.01$) (Table 6). The relationship between the amount of pores and organic matter and silt was remarkably inversely correction ($P < 0.01$), and was remarkably direct associated with bulk density and sand content ($P < 0.01$) (Table 7).

Table 6. Correlation analysis between the total number of aggregates and soil physicochemical properties

Factor	Soil organic	Mechanical composition	Bulk density		
		Sand	Silt	Clay	
correlation index	-0.804**	0.801**	-0.850**	-0.652**	0.178
significance level	0.000	0.000	0.000	0.002	0.453

Notes: ** express the 1% significance level, * express the 5% significance level

Table 7. Correlation analysis between the total number of pore and soil physicochemical properties

Factor	Soil organic	Mechanical composition	Bulk density		
		Sand	Silt	Clay	
correlation index	-0.763**	0.576**	-0.638**	-0.423	0.644**
significance level	0.000	0.008	0.002	0.063	0.002

Notes: ** express the 1% significance level, * express the 5% significance level.

The main power in rainfall erosion is raindrop splash, which causes soil dispersion and saltation on the surface (Wu & Zhou, 1991). Meanwhile, the distribution of splashed soil aggregate particle size will be affected by the aggregate size distribution of undisturbed soil (Wang et al., 2018). In soil erosion experiments, the soil aggregate breakdown caused by raindrop splash may be a major factor affecting the distribution of sediment particle size (Hairsine et al., 1999). In Cumulic Haplustoll, Ustalf and Eum-Orthic Anthrosol, the number of macroaggregates decreased with increasing raindrop diameter, whereas microaggregates showed the opposite trend. This indicates that the degree of fragmentation and decomposition of macroaggregates into microaggregates increased with increasing rainfall erosivity, and larger raindrops led to a greater degree of decomposition, the research of Li et al. (2018) and Fu et al. (2016) also have coincident conclusions. Under the same rainfall conditions, microaggregates were more spherical than macroaggregates. In other words, among the surface soil aggregates, microaggregates were the most numerous, and their shape was the closest to spherical. Generally, soils containing finer aggregates exhibit higher migration ability of pre-separated substances than soils containing larger aggregates (Arjmand Sajjadi & Mahmoodabadi, 2015). This relationship indicates that under rainfall, microaggregates are easier to transport than macroaggregates and can be suspended or deposited in the process of soil water erosion (Li et al., 2018). Subsequent surface soil pore plugging creates the conditions for the formation of soil surface crust. In addition, soils with larger aggregates have higher infiltration rates because such soils are less sensitive to crust formation (Arjmand Sajjadi & Mahmoodabadi, 2015). Therefore, under raindrop splash, Ustochnept and Quartisamment more easily form surface crust, resulting in a reduced infiltration rate and increased runoff.

Under different rainfall conditions, the relative porosity was greatest in macropores (Figure 9B), and macropores were more elongated than small pores. Thus, among the surface soil pores, compared to the porosity of other pore shapes, the elongated pores (>1000 μ m) showed much higher porosity (Figure 9B & Figure 11). The influence of raindrop diameter upon the macropores (> 100 μ m) were significant ($P < 0.05$). Particularly after splashing by 4.05 mm raindrops, the connectivity of the macropores decreased notably (Figure 4). This indicates that after raindrop splashing, the decrease in porosity of elongated

pores and macropores is one of the main reasons for pore plugging. This finding is coincident with the study results of Yang et al. (2020). In the surface pores of Ustalf, they found that before and after raindrop splashing, the elongated pores accounted for 83.93% of the total imaged porosity on average, which make up the primary morphology of soil pores (Yang et al., 2020). Moreover, boosting the relative porosity of elongated pores and macropores can make soil connectivity better, which is more favorable to store water and interchange gas in polyporous medium (Pagliai et al., 2004; Vandenbygaart, Protz, & Tomlin, 1999). The higher the infiltration rate of soil water and solutes, and the more stable the soil structure (Flury & Flühler, 1994).

4.2 Microstructure characteristics of soil under different rainfall conditions

During rainfall, the aggregates were broken by the outside force due to the raindrops hitting the soil surface. The particle size of soil aggregates changed with the fragmentation of aggregates. Microaggregates increased with the increase of raindrop diameter (Figure 3), and then migrated and transported on the soil surface. Subsequently, these migrated aggregates partially enter the surface pores, reducing the surface soil porosity, and finally forming the surface crust. The aggregate and pore structures of Quartisamment and Ustochnept are quite different from those of Cumulic Haplustoll, Ustalf and Eum-Orthic Anthrosol, which are mainly composed of microaggregates with regular shapes. Both of the former soils have fewer macroaggregates (Figure 2 & Figure 3), and the content of $> 250 \mu\text{m}$ macroaggregates can represent the soil anti-erodibility, which increases with the increase of macroaggregates (Mbagwu, 1990). And both of the former soils have low macropore connectivity, the macropores were mostly isolated pores, particularly when the raindrop diameter arrived at 4.05 mm. The reason for this result may be that under rainfall, fine aggregates which are close to spherical shape are more likely to transport with water, and enter the surface soil macro-pores, resulting in pore plugging. Ustochnept and Quartisamment containing more sand (Table 1). These results show that the anti-erodibility of Cumulic Haplustoll, Ustalf and Eum-Orthic Anthrosol is stronger, especially for the Eum-Orthic Anthrosol. Under splashing, fine sand has the least resistance (Ellison, 1947). Therefore, the higher the sand content, the more serious the fragmentation and decomposition of the aggregates (Baver, 1966). The sand content directly affects soil permeability and porosity, thereby affecting soil erodibility (Huaduan & Yingming, 2009). In the soil erosion process, aggregate breakdown and dispersion will affect soil porosity, make the infiltration rate and water conductivity rate reduce, then increase the formation of surface crust and the sensitivity of erosion. At the same time, for the saturated hydraulic conductivity, the soil antecedent water content, bulk density and the constituents of clay are important influencing factors (Zhang et al., 2020). Moreover, for Ustochnept and Quartisamment, there are no macroaggregates $> 500 \mu\text{m}$. This may be related to the low organic matter and clay contents (Table 1), poor adhesion of macroaggregates (Fu et al., 2017a), and few macroaggregates formed by fine particles (Wang et al., 2018).

Both the stability of soil aggregates and the structural properties of soils can be represented and reflected by 3D mass fractal dimension (Gong & Yu Rong, 2001). In the experiment, the 3D FD was adopted to represent the microstructural feature of soil aggregates. The 3D FD can signify the geometric fractal characteristics, self-similar feature and scale independence (Dal Ferro et al., 2013). Accordingly, the lower the 3D FD is, the better the aggregate structure is, and the stronger the soil stability and erosion resistance are (Jing & Zhao, 2009). The FD of each soil increased compared with that of unsplashed soil under splashed by raindrop size of 3.39mm, this shows that soil anti-erodibility decreased via raindrop splash. The stability of soil aggregates has been used to characterize soil anti-erodibility and soil quality (Ghadiri et al., 2007). The FD of Eum-Orthic Anthrosol, Ustalf and Cumulic Haplustoll were lower than those of Quartisamment and Ustochnept. It showed that the structure of Eum-Orthic Anthrosol, Ustalf and Cumulic Haplustoll are more stable. Soil physicochemical properties may explain this phenomenon. The cementation of organic matter on microaggregates is an important mechanism for the formation of macroaggregates. The clay content affects the soil porosity, permeability, cohesion and internal friction angle, thereby affecting the soil anti-erodibility and wash resistance of the soil (Huaduan & Yingming, 2009). The results of Haghghi, Gorji, & Shorafa (2010) also showed that the aggregate stability and hydraulic characteristics of soil could be improved through the retention of organic matter. The stability also increases with increasing clay content of soil (Lado, 2004).

5 Conclusions

Under raindrop splash, the influence of soil type and raindrop diameter upon the total number of aggregates and pores were significant ($P < 0.05$). Under the same rainfall conditions, the number of pores was higher than the number of aggregates. After raindrop splash, as raindrop diameter increased, the number of microaggregates ($> 250 \mu\text{m}$) in Cumulic Haplustoll, Ustalf and Eum-Orthic Anthrosol; the irregular pore-shape factor of Quartisamment and Ustochnept and the total number of aggregates and pores also increased. Under raindrop splash, the soil structure of Eum-Orthic Anthrosol, Ustalf and Cumulic Haplustoll were more stable, Quartisamment and Ustochnept more readily formed a surface crust, resulting in a lower infiltration rate and increased runoff.

The changes in surface aggregates and pore microstructure under rainfall erosion are discussed, which provides a theoretical basis for understanding the soil erosion transport mechanism, water and soil conservation and ecological restoration on the Loess Plateau.

Acknowledgments

We thank the image technology that comes from Shanghai Synchrotron Radiation Facility, Shanghai Institute of Applied Physics, Chinese Academy of Sciences. The National Natural Science Foundation of China (grant number 41571262) supported this work.

References

- Rabot, E. Wiesmeier M. Schluter S. Vogel H. J. (2018), Soil structure as an indicator of soil functions: A review. *Geoderma*, 314, 122-137. doi: 10.1016/j.geoderma.2017.11.009.
- Arjmand Sajjadi, S., & Mahmoodabadi, M. (2015), Aggregate breakdown and surface seal development influenced by rain intensity, slope gradient and soil particle size. *Solid Earth*, 6(1), 311-321. doi:10.5194/se-6-311-2015.
- Angers, D. A., & Caron, J.(1998), Plant-induced changes in soil structure: processes and feedbacks. *Biogeochemistry*, 42(1-2), 55-72. doi: 10.1023/A:1005944025343.
- Baver, L. D. (1966), Soil physics. New York: John Wiley and Sons.
- Beare, M. H., Hendrix, P. F., & Coleman, D. C.(1994), Water-stable aggregates and organic matter fractions in conventional- and no-tillage soils. *Soil Science Society of America Journal*, 58(3). doi: 10.2136/sssaj1994.03615995005800030020x.
- Bissonnais, Y. L. (1996), Aggregate stability and assessment of soil crustability and erodibility.1. Theory and methodology. *European Journal of Soil Science*, 47(4), 425-437. doi: 10.1111/j.1365-2389.1996.tb01843.x.
- Dal Ferro, N., Charrier, P., & Morari, F. (2013), Dual-scale micro-CT assessment of soil structure in a long-term fertilization experiment. *Geoderma*, 204, 84-93. doi:10.1016/j.geoderma.2013.04.012.
- Dimitrova, R. S., & Yanful, E. K. (2012), Factors affecting the shear strength of mine tailings/clay mixtures with varying clay content and clay mineralogy. *Engineering Geology*, 125, 11-25. doi: 10.1016/j.enggeo.2011.10.013.
- Ekwue, E. I. (1991), The effects of soil organic matter content, rainfall duration and aggregate size on soil detachment. *Soil Technology*, 4(3), 197-207. doi: 10.1016/0933-3630(91)90001-4.
- Ellison, W.D. (1947), Soil Erosion Studies—Part I. *Agricultural Engineering*, 28, 145-146.
- Flury, M., & Flühler, H. 1994. Brilliant blue fcf as a dye tracer for solute transport studies—a toxicological overview. *Journal of Environmental Quality*, 23(5). doi: 10.2134/jeq1994.00472425002300050037x.
- Fu, Y., Li, G. L., Zheng, T. H., Li, B. Q., & Zhang, T. (2016), Impact of raindrop characteristics on the selective detachment and transport of aggregate fragments in the Loess Plateau of China. *Soil Science Society of America Journal*, 80(4), 1071-1077. doi:10.2136/sssaj2016.03.0084.
- Fu, Y., Li, G. L., Zheng, T. H., Li, B. Q., & Zhang, T. (2017a), Splash detachment and transport of loess aggregate fragments by raindrop action. *Catena*, 150, 154-160. doi:10.1016/j.catena.2016.11.021.

- Fu, Y., Li, G. L., Zheng, T. H., Li, B. Q., & Zhang, T. (2017b), Effects of rain-drop splash on aggregate particle size distribution of soil plough layer. *Transactions of the Chinese Society of Agricultural Engineering*, 33(3), 155-160. doi: 10.11975/j.issn.1002-6819.2017.03.021.
- Fu, Y., Li, G. L., Zheng, T. H., Zhao, Y. S., & Yang, M. X. 2020. Fragmentation of soil aggregates induced by secondary raindrop splash erosion. *Catena*, 185. doi:10.1016/j.catena.2019.104342.
- Fu, Y., Yang, M. X., Li, G. L., Wang, D., & Zheng, T. H. 2020. Selectivity of aggregate fractions for loess soils under different raindrop diameters. *Journal of Soils and Sediments*. doi:10.1007/s11368-020-02740-x.
- Garbout, A., Munkholm, L. J., & Hansen, S. B. (2013), Temporal dynamics for soil aggregates determined using X-ray CT scanning. *Geoderma*, 2045, 15-22. doi:10.1016/j.geoderma.2013.04.004.
- Garbout, A., Munkholm, L. J., Hansen, S. R. B., Petersen, B. R. M., Munk, O. L., & Pajor, R. (2012), The use of PET/CT scanning technique for 3D visualization and quantification of real-time soil/plant interactions. *Plant & Soil*, 352(1-2), 113-127. doi:10.1007/s11104-011-0983-8.
- Ghadiri, H., Hussein, J., & Rose, C. W. (2007), A study of the interactions between salinity, soil erosion, and pollutant transport on three Queensland soils. *Soil Research*, 45(6), 404-413. doi: 10.1071/SR07038.
- Gong, A. D. & Yu-Rong, H. E. (2001), Study on fractal features of soil structure of degraded soil in dry and hot valley region of jinsha river. *Journal of Soil Water Conservation*, 015(003), 112-115. doi: CNKI:SUN:TRQS.0.2001-03-028.
- Haghighi, F., Gorji, M., & Shorafa, M. (2010), A study of the effects of land use changes on soil physical properties and organic matter. *Land Degradation & Development*, 21(5), 496-502. doi: 10.1002/ldr.999.
- Hairsine, P. B., Sander, G. C., Rose, C. W., Parlange, J. Y., Hogarth, W. L., Lisle, I., & Rouhipour, H. (1999), Unsteady soil erosion due to rainfall impact: a model of sediment sorting on the hillslope. *Journal of Hydrology*, 220(3-4), 115-128. doi:10.1016/s0022-1694(99)00068-2.
- Hu, W., Zheng, F. L., & Bian, F. (2016), The directional components of splash erosion at different raindrop kinetic energy in the Chinese Molisol region. *Soil Science Society of America Journal*, 80(5), 1329-1340. doi:10.2136/sssaj2016.03.0066.
- Gao, H. D., & Liu, Y. M. (2009), Impact of ground substance on mechanical composition of soil in Guizhou Province. *Science of Soil and Water Conservation*, 6. doi: 10.16843/j.sswc.2009.06.010.
- Jiao, J. (1999), Precipitation and erosion characteristics of rain-storm in different pattern on Loess Plateau. *Journal of arid land resources and environment*, (1), 34-42. doi: 10.1088/0256-307X/15/12/025.

- Jing, S. U. , & Zhao, S. W. (2009), Comparison of the analysis methods for soil aggregate stability. *Bulletin of Soil and Water Conservation*. doi: 10.13961/j.cnki.stbctb.2009.05.024.
- Lado, M.(2004), Soil wetting and texture effects on aggregate stability, seal formation, and erosion. *Science Society of America Journal*, . doi: 10.2136/sssaj2004.1992.
- Lado, M., Paz, A., & Ben-Hur, M. (2004), Organic matter and aggregate-size interactions in saturated hydraulic conductivity. *Soil ence Society of America Journal*, 68(1), 234-242. doi: 10.2136/sssaj2004.2340.
- Lars J. Munkholm , R. J. H., BillDeen,T.Zidar.2016. Relationship between soil aggregate strength, shape and porosity for soils under different long-term management. *Geoderma*. doi:10.1016/j.geoderma.2016.01.005.
- Legout, C., Leguedois, S., Le Bissonnais, Y., & Issa, O. M. (2005), Splash distance and size distributions for various soils. *Geoderma*, 124(3-4), 279-292. doi:10.1016/j.geoderma.2004.05.006.
- Li, G. L., & Pang, X. M. (2010), Effect of land-use conversion on C and N distribution in aggregate fractions of soils in the southern Loess Plateau, *China. Land Use Policy*, 27(3), 706-712. doi:10.1016/j.landusepol.2009.09.011.
- Li, G. L., & Pang, X. M. (2014), Difference in organic carbon contents and distributions in particle-size fractions between soil and sediment on the Southern Loess Plateau, China. *Journal of Mountain Science*, 11(3), 717-726. doi:10.1007/s11629-013-2757-7.
- Li, G. L., Fu, Y., Li, B. Q., Zheng, T. H., Wu, F. Q., Peng, G. Y., & Xiao, T. Q. (2018), Micro-characteristics of soil aggregate breakdown under raindrop action. *Catena*, 162, 354-359. doi:10.1016/j.catena.2017.10.027.
- Liu, Y. , Wang, S. , Zhang, F. , Yang, Z. , & Wang, R. (2016), Micromorphological characteristics of soil for production base of high quality rose in miaofeng mountain of beijing. *Acta Pedologica Sinica*. doi: 10.11766/trxb201509090324.
- Luxmoore, R. J. (1981), Micro-, meso-, and macroporosity of soil. *Science Society of America Journal*, 45(3). doi: 10.2136/sssaj1981.03615995004500030051x.
- Ma, R. M., Jiang, Y., Liu, B., & Fan, H. M. (2021), Effects of pore structure characterized by synchrotron-based micro-computed tomography on aggregate stability of black soil under freeze-thaw cycles. *Soil & Tillage Research*, 207, 10.1016/j.still.2020.104855.
- Mbagwu, J. , & Piccolo, A. (1990), Carbon, nitrogen and phosphorus concentrations in aggregates of organic waste-amended soils. *Biological Wastes*, 31(2), 97-111. doi: 10.1016/0269-7483(90)90164-N.
- Murphy, C. P. (1987), Thin section preparation of soils and sediments. *Soil Science*, 144(4). doi: 10.1097/00010694-198710000-00013.

- Pagliai, M., Vignozzi, N., & Pellegrini, S. (2004), Soil structure and the effect of management practices. *Soil and Tillage Research*, 79(2), 131-143. doi:10.1016/j.still.2004.07.002.
- Parsons, A. J., Abrahams, A. D., & Wainwright, J. (1994), Rainsplash and erosion rates in an interrill area on semi-arid grassland, Southern Arizona. *Catena*, 22(3), 215-226. doi: 10.1016/0341-8162(94)90003-5.
- Perret, J., Prasher, S., & Kacimov, A. (2003), Mass fractal dimension of soil macropores using computed tomography: from the box-counting to the cube-counting algorithm. *European Journal of Soil Science*, 54(3), 569-579. doi: 10.1046/j.1365-2389.2003.00546.x.
- Qin, Y. , Tu, S. , Wang, Z. , & Feng, W. 2009. Micro-morphological Features of A Purple Soil under Different Long-term Fertilizer Treatments. *Ecology and Environmental Sciences*, 18(001), 352-356. doi: 10.3969/j.issn.1674-5906.2009.01.065.
- Ramos, M. C., Nacci, S., & Pla, I. (2003), Effect of raindrop impact and its relationship with aggregate stability to different disaggregation forces. *Catena*, 53(4), 365-376. doi:10.1016/s0341-8162(03)00086-9.
- Serrano-Muela, M. P., Nadal-Romero, E., Lana-Renault, N., González-Hidalgo, J. C., López-Moreno, J. I., Beguería, S., & García-Ruiz, J. M. (2015), An exceptional rainfall event in the Central Western Pyrenees: spatial patterns in discharge and impact. *Land Degradation & Development*, 26(3), 249-262. doi:10.1002/ldr.2221.
- Starkloff, T., Larsbo, M., Stolte, J., Hessel, R., & Ritsema, C. (2017), Quantifying the impact of a succession of freezing-thawing cycles on the pore network of a silty clay loam and a loamy sand topsoil using X-ray tomography. *Catena*, 156, 365-374. doi: 10.1016/j.catena.2017.04.026.
- Taina, I. A., Heck, R. J., & Elliot, T. R. (2008), Application of X-ray computed tomography to soil science: A literature review. *Canadian Journal of Soil Science*, 88(1), 1-19. doi: 10.4141/CJSS06027.
- Taina, I. A., Heck, R. J., Deen, W., & Ma, E. (2013), Quantification of freeze-thaw related structure in cultivated topsoils. *Canadian Journal of Soil Science*, 93(4), 533-553. doi: 10.4141/CJSS2012-044.
- Vandenbygaart, A. J., Protz, R., & Tomlin, A. D. (1999), Changes in pore structure in a no-till chronosequence of silt loam soils, southern Ontario. *Canadian Journal of Soil Science*, 79(1), 149-160. doi: 10.4141/S98-034.
- Vogel, H. J. (1997), Morphological determination of pore connectivity as a function of pore size using serial sections. *European Journal of Soil Science*, 48(3), 365-377. doi:10.1046/j.1365-2389.1997.00096.x.
- Wang, A. L., Yan, X. L., & Wei, Z. J. (2018), ImagePy: an open-source, python-based and platform-independent software package for bioimage analysis. *Bioin-*

formatics,34(18),3238-3240. doi: 10.1093/bioinformatics/bty313.

Wang, D., Li, G. L., Fu, Y., Gao, G. X., & Zheng, T. H. (2018), Detachment and transport characteristics of sandy loam soil by raindrop action in the northern Loess Plateau, China. *Journal of Soil & Water Conservation*, 73(6), 705-713. doi: 10.2489/jswc.73.6.705.

Wu, P.T., & Zhou, Z.H.(1991), The effect of land slope upon raindrop splash erosion. *Bulletin of Soil & Water Conservation*, 011(003), 8-13. doi: 10.13961/j.cnki.stbctb.1991.03.002.

Wu, X. Y., Yu, X. X., Gao, Y. J., & Wang, G. R. (2017), Different impacts of rainfall intensity on surface runoff and sediment loss between huang-mian soil and brown soil. *Journal Of Environmental Science And Management*, 20(2), 1-8.

Y., Bissonnais, L., & Arrouays, D. (1997), Aggregate stability and assessment of soil crustability and erodibility.2. Application to humic loamy soils with various organic carbon contents. *European Journal of Soil Science*,48(1),39-48. doi: 10.1111/j.1365-2389.1997.tb00183.x.

Yang, M. X., Fu, Y., Li, G. L., Ren, Y. Y., Li, Z. F., & Ma, G. G. (2020), Microcharacteristics of soil pores after raindrop action. *Soil ence Society of America Journal*, 84(5),1693-1704.doi: 10.1002/saj2.20113

Young, I. M., & Crawford, J. W. (2004), Interactions and self-organization in the soil-microbe complex. *Science*, 304 (5677), 1634-1637. doi: 10.1126/science.1097394

Zhang, Y., Zhao, W., Li, X., Jia, A., & Kang, W.(2020), Contribution of soil macropores to water infiltration across different land use types in a desert-oasis ecoregion. *Land Degradation & Development*, 32(4),1751-1760. doi: 10.1002/ldr.3823

Zhao, D., Xu, M., Liu, G., Ma, L., Zhang, S., Xiao, T., & Peng, G. (2017), Effect of vegetation type on microstructure of soil aggregates on the Loess Plateau, China. *Agriculture, Ecosystems & Environment*, 242, 1-8. doi:10.1016/j.agee.2017.03.014

Zhao, D., Xu, M., Liu, G., Yao, X., Tuo, D., Zhang, R., & Peng, G. (2017), Quantification of soil aggregate microstructure on abandoned cropland during vegetative succession using synchrotron radiation-based micro-computed tomography. *Soil and Tillage Research*, 165, 239-246. doi:10.1016/j.still.2016.08.007

Zhou, H., Fang, H., Mooney, S. J., & Peng, X. (2015), Effects of long-term inorganic and organic fertilizations on the soil micro and macro structures of rice paddies. *Geoderma*, 266, 66-74. doi:10.1016/j.geoderma.2015.12.007

Zhou, H., Peng, X., Peth, S., & Xiao, T. Q. (2012), Effects of vegetation restoration on soil aggregate microstructure quantified with synchrotron-based micro-computed tomography. *Soil and Tillage Research*, 124, 17-23.

doi:10.1016/j.still.2012.04.006